Atmospheric Environment 172 (2018) 16–25

Contents lists available at ScienceDirect

Atmospheric Environment

journal homepage: www.elsevier.com/locate/atmosenv

Comparative study of elemental mercury flux measurement techniques over a Fennoscandian boreal peatland

S. Osterwalder[a,b,*,1], J. Sommar[c,1], S. Åkerblom[d], G. Jocher[b], J. Fritsche[a], M.B. Nilsson[b], K. Bishop[d,e], C. Alewell[a]

[a] Department of Environmental Sciences, University of Basel, Basel, Switzerland
[b] Department of Forest Ecology and Management, Swedish University of Agricultural Sciences, Umeå, Sweden
[c] State Key Laboratory of Environmental Geochemistry, Institute of Geochemistry, Chinese Academy of Sciences, Guiyang, China
[d] Department of Aquatic Sciences and Assessment, Swedish University of Agricultural Sciences, Uppsala, Sweden
[e] Department of Earth Sciences, University of Uppsala, Uppsala, Sweden

ARTICLE INFO

Keywords:
Land-atmosphere exchange
Dynamic flux chamber
Micrometeorology
Relaxed eddy accumulation
Elemental mercury

ABSTRACT

Quantitative estimates of the land-atmosphere exchange of gaseous elemental mercury (GEM) are biased by the measurement technique employed, because no standard method or scale in space and time are agreed upon. Here we present concurrent GEM exchange measurements over a boreal peatland using a novel relaxed eddy accumulation (REA) system, a rectangular Teflon® dynamic flux chamber (DFC) and a DFC designed according to aerodynamic considerations (Aero-DFC). During four consecutive days the DFCs were placed alternately on two measurement plots in every cardinal direction around the REA sampling mast. Spatial heterogeneity in peat surface characteristics (0–34 cm) was identified by measuring total mercury in eight peat cores (57 ± 8 ng g^{-1}, average ± SE), vascular plant coverage (32–52%), water table level (4.5–14.1 cm) and dissolved gaseous elemental mercury concentrations (28–51 pg L^{-1}) in the peat water. The GEM fluxes measured by the DFCs showed a distinct diel pattern, but no spatial difference in the average fluxes was detected (ANOVA, $\alpha = 0.05$). Even though the correlation between the Teflon® DFC and Aero-DFC was significant ($r = 0.76$, $p < 0.05$) the cumulative flux of the Aero-DFC was a factor of three larger. The average flux of the Aero-DFC (1.9 ng m^{-2} h^{-1}) and REA (2 ng m^{-2} h^{-1}) were in good agreement. The results indicate that the novel REA design is in agreement for cumulative flux estimates with the Aero-DFC, which incorporates the effect of atmospheric turbulence. The comparison was performed over a fetch with spatially rather homogenous GEM flux dynamics under fairly consistent weather conditions, minimizing the effect of weather influence on the data from the three measurement systems. However, in complex biomes with heterogeneous surface characteristics where there can be large spatial variability in GEM gas exchange, the small footprint of chambers (< 0.2 m^2) makes for large coefficients of variation. Thus many chamber measurement replications are needed to establish a credible biome GEM flux estimate, even for a single point in time. Dynamic flux chambers will, however, be able to resolve systematic differences between small scale features, such as experimentally manipulated plots or small scale spatial heterogeneity.

1. Introduction

Globally, anthropogenic mercury (Hg) emissions to the atmosphere and its subsequent deposition have increased the storage of this neurotoxic element in peat by a factor of ~4 since pre-industrial times (Amos et al., 2015). The semi-volatile elemental form is produced in organic soils by a suite of reductive (photochemical, microbial, and dark abiotic) processes from the Hg^{2+} pool and can be re-emitted to the atmosphere. The quantification of gaseous elemental mercury (GEM) fluxes from terrestrial environments is important, because the re-emission of GEM to the atmosphere converts the soil bound and rather immobile Hg into a mobile form with potential long-range transport (Selin et al., 2008) subsequent deposition, and accumulation in food chains.

Two main methodologies exist to measure land-atmosphere exchange of GEM: First, dynamic flux chambers (DFCs) representing small-scale spatial measurements which are ideal for comparison studies to understand the influence of individual controlling factors on

* Corresponding author. University of Basel, Bernoullistrasse 30, 4056 Basel, Switzerland.
E-mail address: stefan.osterwalder@unibas.ch (S. Osterwalder).
[1] These authors wish to be considered joint first authors.

http://dx.doi.org/10.1016/j.atmosenv.2017.10.025
Received 15 June 2017; Received in revised form 3 October 2017; Accepted 9 October 2017
Available online 14 October 2017

GEM flux (Gustin et al., 1999). The method is based on GEM concentration measurements between the inlet and outlet of the DFC. Up to now DFCs have been used for 85% of GEM flux measurements (Agnan et al., 2016). However, DFC measurements have been criticized because the enclosure disturbs the microclimate by influencing aerodynamics, temperature and the radiation balance (Wallschläger et al., 1999; Gustin et al., 1999). Furthermore, a high variability was observed among DFC studies due to differences in designs, operating procedures, and application protocols (Eckley et al., 2010), as well as a limited spatial representativeness (as reviewed by Agnan et al., 2016).

To overcome the limitation of the DFC measurements, micrometeorological methods (MM) have been developed which allow larger spatial-scale measurements and only marginally modify environmental conditions. They include the relaxed eddy accumulation (REA) method (Cobos et al., 2002; Olofsson et al., 2005; Bash and Miller, 2008; Sommar et al., 2013; Osterwalder et al., 2016; Kamp et al., 2017), the aerodynamic gradient (AGM) methods (e.g. Lindberg et al., 1995; Edwards et al., 2005; Fritsche et al., 2008b; Baya and Van Heyst, 2010), and the modified Bowen ration (MBR) method (e.g. Obrist et al., 2006; Fritsche et al., 2008b; Converse et al., 2010). Field trials of Hg eddy covariance (EC) measurements over background sites revealed no manifest GEM-vertical wind covariance, indicating fluxes were below the method detection limit (Pierce et al., 2015). Comparison studies over Hg-enriched soils have shown that fluxes determined with DFCs were nearly three times lower compared to fluxes derived from AGM and MBR method fluxes (Wallschläger et al., 1999; Gustin et al., 1999; Zhu et al., 2015a). Carpi and Lindberg (1997) found that MM-derived fluxes were generally up to 20% higher than DFC fluxes for sludge-amended soils and Pierce et al. (2015) reported 16% lower fluxes measured with a DFC compared to MBR fluxes. A new type of dynamic flux chamber (Aero-DFC) designed by Lin et al. (2012) accounts for atmospheric surface-layer shear properties by a scaling procedure. Field comparisons indicated that Aero-DFC may bridge the gap in magnitude between DFC- and MM-derived fluxes. Aero-DFC differed less than 10% from AGM and MBR, while the flux derived from a traditional DFC was 42% and 31% lower compared to AGM and MBR (Zhu et al., 2015a).

The choice of methods to capture GEM fluxes depends on availability of resources as well as expert knowledge. While DFC measurements are relatively low-cost and require only medium expert knowledge, MM methods and especially the REA method are highly cost intensive and require long-term availability of highly specialized staff. The question remains if DFC measurements can still deliver valuable quantitative GEM flux estimates, where MM methods are not feasible.

Due to the different scales associated, a comparison of DFC (surface area of typically < 0.1 m^2) to MM methods (hundreds to thousands of m^2 or more) has to consider the site heterogeneity. The peatland surface within the footprint of an EC system operating at Degerö Stormyr in northern Sweden has previously been defined as a homogeneous mixture of wet lawns and carpet plant communities (Nilsson et al., 2008). Nevertheless, the GEM source strength could be altered by spatial changes in total Hg concentrations in the peat (THg), abundance of vascular plants (VP), water table level (WTL), or dissolved gaseous Hg (DGM) concentration in peatland pore water. Correlations between THg in the soil and GEM fluxes have been found across individual background sites (Nacht and Gustin, 2004; Sigler and Lee, 2006). Higher abundance of vascular plants is expected to contribute more to GEM re-emission due to less Hg sequestration compared to bryophytes (Selvendiran et al., 2008) as well as the capacity of DGM transport by transpiration flow and release of GEM through stomata (Lindberg et al., 2002). Water bodies are defined as net sources of GEM to the atmosphere (Wang et al., 2014). Thus, high water table levels and elevated concentrations of volatile DGM, especially during periods of high surface wind speeds, may promote GEM emissions leading to small scale spatial variability of Hg fluxes to the atmosphere.

The objective of this study was to investigate whether DFC and REA measurements are comparable if small-scale variation in the GEM flux was accounted for by spatial repetition of DFC measurements. As such, the integrated GEM flux over a larger spatial extension upwind of a REA sampling mast at Degerö Stormyr was compared with simultaneous GEM fluxes determined over spatially repeated small footprints using a pair of co-located TDFC and Aero-DFC. We compared and evaluated quantitatively derived GEM fluxes from REA and two different DFC designs, which is a contribution to method standardization. Thus, we present the first method comparison between a Teflon® perfluoroalkoxy (PFA) DFC (TDFC), an Aero-DFC and a dual-inlet, single detector REA system deployed at a pristine peatland catchment site in northern Sweden. Peatlands are hot spots in the landscape for production of highly toxic methylmercury (MeHg) species that in-turn biomagnifies in aquatic food webs. This makes investigations of Hg cycling in such environments of considerable interest (St. Louis et al., 1994; Mitchell et al., 2008; Bergman et al., 2012). GEM land-atmosphere exchange studies conducted over northern peatlands are scarce, but indicated that wetland GEM evasion may seasonally rival the input flux of Hg wet deposition (e.g. Kyllönen et al., 2012; Fritsche et al., 2014; Osterwalder et al., 2016).

2. Material and methods

2.1. Site description

Measurements were performed continuously between July 8 and 12, 2014 in the center of Degerö Stormyr (2.7 km^2), a mixed acid mire system (64°11′N, 19°33′E; 270 m a.s.l.) situated in the Kulbäcksliden domain of the Svartberget long-term experimental research (LTER) facility near Vindeln in the county of Västerbotten, northern Sweden. The surrounding forest is a mixed coniferous forest (*Pinus sylvestris* L. and *Picea abies* L. H. Karst) with minor contribution by birch (*Betula pubescens* Ehrh.). Forested areas in the proximity to the Eddy Covariance and REA flux tower are marked green in Fig. 1a. A LiDAR-derived digital elevation model and aerial photo of the entire catchment can be reviewed in Leach et al. (2016). The average peat depth is between 3 and 4 m. The deepest organic layers correspond to an age of ~8000 years. The peat THg concentrations between 0 and 34 cm measured in autumn 2015 averaged 57 ± 8 (± SE) ng g^{-1}. These levels are consistent with the designation of this area as a background site in the boreal zone. Vegetation cover within the REA fetch mainly consists of vascular plants (dominated by *Eriophorum vaginatum* L., *Trichophorum cespitosum* L. Hartm., *Vaccinium oxycoccos* L., *Andromeda polifolia* L., and *Rubus chamaemorus* L., sparsely interspersed with *Carex limosa* L., and *Schezeria palustris* L.) and Sphagnum species (*Sphagnum majus* Russ. C. Jens, *S. lindbergii* Schimp., *S. balticum* Russ. C. Jens, *S. fuscum* Schimp.Klinggr. and *S. rubellum* Wils) (Nilsson et al., 2008; Laine et al., 2012). The 30 year (1981–2010) mean annual precipitation and temperature are 614 mm and +1.8 °C respectively, while the mean temperature in July is +14.7 °C (Ottosson-Löfvenius et al., 2003; Laudon et al., 2013). The dominant wind-direction in summer is northeast (Sagerfors et al., 2008).

2.2. Relaxed eddy accumulation technique

The dual-inlet, single detector REA system consists of a USA-1 ultrasonic anemometer (METEK GmbH, Elmshorn, Germany) to measure standard deviation of the vertical wind velocity, two sets of fast-response valves (Model 6128, Bürkert, Ingelfingen, Germany) to sample and separate vertically upward and downward moving air parcels, GEM adsorption cartridges, an atomic fluorescence analytical unit (Tekran Model 2500, Toronto, Canada) as well as a GEM reference gas and Hg zero-air generator unit. The REA design and operation parameters are described in detail by Osterwalder et al. (2016). The vertical GEM flux is calculated over 30 min intervals using:

$$F_{REA} = \beta \sigma_w (\overline{C_u} - \overline{C_d}), \quad (1)$$

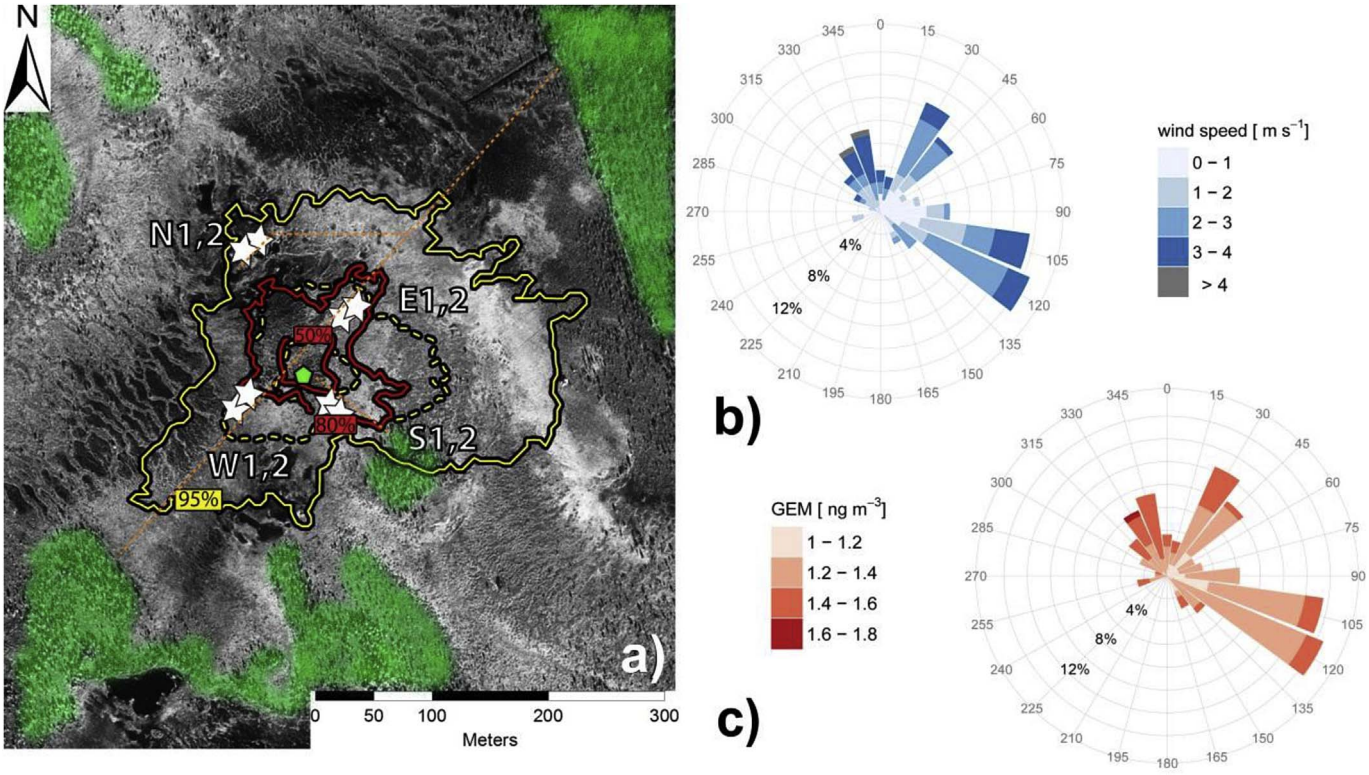

Fig. 1. (a) Aerial photograph of Degerö Stormyr with contour lines indicating the predicted source area of GEM flux measured by the relaxed eddy accumulation (REA) system. The green polygon marks the location of the REA sampling mast. The footprint of the innermost red circle corresponds to 50% of the measurements performed during the four-day campaign. The second red circle includes 80% of the measurements. The yellow contours (50% and 80% dashed line, 95% continuous line) indicate the source area of the measurements for the period from 02.07 to 17.07.2014). Locations of the eight plots for the DFC measurements are shown as white stars arranged in all four cardinal directions. Forested areas are highlighted in green. The polar histogram for (b) wind speed and (c) air GEM concentration describe the conditions during the campaign. Source of the aerial photograph: GSD-Orthofoto IR © Swedish Mapping, Cadastral and Land Registration Authority (2004). (For interpretation of the references to colour in this figure legend, the reader is referred to the web version of this article.)

where σw is the standard deviation of the vertical wind velocity, $\overline{C_u} - \overline{C_d}$ is the difference between the average GEM concentration in updrafts and downdrafts, respectively and β is the relaxation coefficient determined by assuming the EC sensible heat flux (see Sect. 2.2) equal to corresponding REA flux derived analogous to Equation (2):

$$\beta = \frac{\overline{w'T'}}{\sigma_w(\overline{T_u} - \overline{T_d})}, \tag{2}$$

where $\overline{T_u} - \overline{T_d}$ is the difference between averaged air temperatures measured in updrafts and downdrafts, respectively. A zero centered dynamic deadband (0.5σw) was introduced. A recursive high-pass filter removed bias in measurements from vertical wind velocity (McMillen, 1988; Richardson et al., 2012). GEM recovery was monitored by automated and alternate injections (every 30 min) of a GEM reference gas and dry Hg-free air.

REA raw flux data were post-processed by implementing a series of standard corrections and by applying rejection criteria following Osterwalder et al. (2016). 8% of the 30-min data were discarded. The gaps were filled for better comparability with DFC fluxes using a look-up table where 6 fixed intervals for air temperatures between 5 and 35 °C were defined. Air temperature showed a light but significant correlation with the REA flux ($r = 0.26$, $p < 0.05$) and was recorded continuously during the campaign. Before and after the measurement campaign the system was set to operate in a reference mode to check for up- and downdraft sampling line bias. Based on the performance in reference mode, the detection limit was derived in two steps by (i) calculating the GEM concentration difference between the two gold cartridge pairs and by (ii) resolving the absolute standard deviation of the residuals from orthogonal regression fitting (cf. Zhu et al., 2015b).

2.3. Enclosure techniques

Two types of DFCs were deployed in side-by-side measurements. The TDFC with a square footprint (0.44 m × 0.44 m) was made of 0.25 mm Teflon® PFA film supported by a rectangular frame (height: 0.29 m). The TDFC has five 1 cm diameter holes at regular distances along each of the four sidewalls aligned horizontally 6 cm above the ground surface. The sample port (Ø 0.5 cm) was located in the top and center of the DFC (see Fig. S1a in the supplementary material). The characteristics and performance of the polycarbonate Aero-DFC has previously been documented in Lin et al. (2012) and Zhu et al. (2015a, b). The measurement zone of Aero-DFC covering a surface of 0.09 m^2 and the design produces a uniform surface friction velocity here that can be controlled by the sampling flow rate. Therefore, the flux under atmospheric conditions can be derived from measured flux normalized by the ratio of the overall mass transfer coefficient in ambient air to that in the Aero-DFC (Eq. (4)). Both DFCs were operated at a flow rate of 13.3 L min^{-1} corresponding to turnover times of 4.2 min and 0.4 min for TDFC and Aero-DFC, respectively. The TDFC flux was calculated according to Equation (3) (Xiao et al., 1991) and the Aero-DFC flux determined with Equation (4), incorporating surface shear properties (Lin et al., 2012):

$$F_{TDFC} = \frac{Q(C_i - C_o)}{A_{TDFC}}, \tag{3}$$

$$F_{Aero-DFC} = \frac{Q(C_i - C_o)}{A_{Aero-DFC}} \cdot \frac{\left(4.86 + \frac{0.03h^2u_*D_H/(6kz_0Dl)}{1+0.016\sqrt[3]{\{(h^2u_*D_H)/(6z_0Dl)\}^2}}\right)}{\left(4.86 + \frac{0.03hQD_H/(A_cDl)}{1+0.016\sqrt[3]{\{(hQD_H)/(A_cDl)\}^2}}\right)}, \tag{4}$$

where F_{TDFC} and $F_{AERO\text{-}DFC}$ are the GEM fluxes derived from the TDFC and Aero-DFC method, respectively, Q is the applied flow rate

(13.3 L min^{-1}), C_i and C_o are the inlet and outlet GEM concentrations, respectively and A is the surface enclosed by the DFCs. h is the height of the flow channel (0.03 m). The length of the Aero-DFC body is 0.7 m and divided into three zones, the entrance (0.3 m), measurement (0.3 m) and exit zone (0.1 m). The midpoint of the measurement zone is designated as l (0.15 m), u^* is the friction velocity, k is the Kármán constant, z_0 is surface roughness height, A_c is the flow cross-sectional area (0.009 m^2) and D_H and D are the hydraulic radius (0.0545 m) and diffusivity of GEM ($1.194 \cdot 10^{-5}$ m^2 s^{-1}), respectively (please note that a picture of the Aero-DFC is shown in Fig. S1b in the supplementary material).

Prior to application in the field, the DFCs were cleaned in a 5% nitric acid bath for 24 h and rinsed with ultrapure water (Milli-Q, 18.2 MΩ cm, Millipore Corp.). Blank measurements were performed on site over an acid-cleaned Teflon® PTFE film before and after the campaign. The blanks calculated for TDFC (0.1 ± 0.2 ng m^{-2} h^{-1}, n = 51) and Aero-DFC (0.3 ± 0.3 ng m^{-2} h^{-1}, n = 115) were interpolated and subtracted from the calculated GEM fluxes. Typical sources of uncertainty for REA and DFC measurements were reviewed in Zhu et al. (2015b).

2.4. Instrumentation and sampling

The anemometer and intake lines of the REA system were installed 3.5 m above the surface. The former measured turbulent fluctuations of the horizontal and vertical wind at a resolution of 20 Hz. 30 min averages of horizontal wind speed, wind direction, friction velocity (u*) and stability (z/L) were derived. EC systems with sensors installed 15 m north of the REA sampling mast have been measuring exchange of greenhouse gases, water vapor and energy at 1.8 m height a.g.l. since 2001 (Sagerfors et al., 2008) and since 2013 within the Pan-European Integrated Carbon Observation System (ICOS) infrastructure. From these measurements 30 min averages of the sensible heat flux were derived for β-calculations (Eq. (2)). Sensors to measure additional climate variables were placed on the same mast (see details below). 8.5 m long Teflon® PFA sampling tubes connected the fast-response valves with the GEM-accumulation and analysis system. The system was installed in a temperature controlled dome shaped plexiglass container (Igloo Satellite Cabin, Icewall One, Australia), which also houses the main part of the ICOS instrumentation.

The REA footprint was estimated for each half-hour period during the campaign and beyond (July 2–17, 2014) using a Lagrangian stochastic forward model (Rannik et al., 2000) based on atmospheric conditions, measurement height and surface roughness (0.02 m, Sagerfors et al., 2008). Footprint modeling is crucial to pin-point overlap between the source area of REA flux and the DFC measurement plots. These plots are located within 65 m of the REA sampling mast in E, S and W direction. The N plots are more distant (~120 m) from the REA sampling mast (Fig. 1a).

The ground based, mobile DFC sampling setup consisted of the additional coupling units of a flushing system, a two port sampling valve system and an automated Hg vapor analyzer (see further details in Fig. S1c in the supplementary material). Alternately, in 1 h intervals the DFCs were deployed over two plots at every cardinal direction. In clockwise direction, the DFC measurements started at the plots in the north and were rotated for four full laps during the campaign. At the inlet and outlet of the DFCs, a sub-stream of air (1.3 L min^{-1}) was sequentially sampled twice at 5 min intervals using a Synchronized Two-Port Sampler (Tekran Model 1110, Toronto, Canada). Plot specific 1 h GEM fluxes were calculated using Equations (3) and (4) for TDFC (n = 32) and Aero-DFC (n = 32), respectively. The measurements were evenly distributed over the 4 days in order to be comparable with the 30 min REA fluxes (n = 192). Boardwalks gave access to all measurement plots and guaranteed an undisturbed investigation of the peatland surface. After every measurement, the DFCs were cleaned with ultrapure water and air dried. 15 min prior to sampling the DFCs were put on the plots again. The DFC and REA Hg analyzers (Tekran Model 2537A and 2500, respectively) were calibrated in-situ before and after the field campaign using a temperature-controlled Hg vapor calibration unit (Tekran Model 2505). Multiple volumes (3–8 μl) of saturated GEM vapor were manually injected into a Hg-free air stream obtained from a zero-air generator (Tekran Model 1100) using a 10 μl digital gas-tight syringe (Hamilton, Reno, USA). Dry deposition velocities were calculated for the REA and DFC method by dividing the GEM flux by the air GEM concentration measurements at the same height (Poissant et al., 2004). Statistical calculations were performed using R version 3.1.2 (R Development Core Team, 2011).

2.5. Environmental parameters

Eight peat cores (0–34 cm) were taken in autumn 2015 close to the plots where GEM flux measurements were performed. The cores were cut in 2 cm increments, air-dried and sieved (< 2 mm). THg analysis was performed by thermal decomposition (750 °C) followed by amalgamation on gold-traps, thermal desorption, and analysis of vapor Hg by Atomic Absorption Spectroscopy according to EPA method 7473. Certified reference lake sediment material (IAEA SL-1) was used for calibrations. Replicate samples and the reference material were analyzed regularly (10% of the sampling sequence) with an established precision of < 3% (relative SD).

On the eight measurement plots, vegetation composition was investigated using percent cover estimates following Wiedermann et al. (2007). The flat area within the plots was representative for the REA footprint and was fully covered by Sphagnum. Vascular plants growing within the plots were dominated by sedges and dwarf-shrubs. The vascular plant coverage was calculated for each plot.

Water table levels were determined after every DFC measurement (n = 64) using basic plumbing well-tubes (Ø 16 mm) drilled into the peat next to the plots. A standard procedure was applied by inserting a scaled PVC-tube into the wells and blowing into it until a bubbling was heard.

To determine peat water DGM concentrations, surface water samples (collected at WTL-10 cm) were collected in a 1 L PFA vessel and analyzed immediately in the field using an automated purging system following Lindberg et al. (2000). The samples were purged with Hg-free air (Tekran Model 1100) for a total of 60 min (40 min sample, 20-min whole-blank) at a flow rate of 1.2 L min^{-1}. The DGM concentration was then calculated from the difference between the sample and blank (1.3 ± 0.8 pg) purges and was expressed on a water volume basis. Between the single measurements the vessel was purged with ultrapure water for 20 min. DGM in ultrapure water was always below the detection limit of ~0.5 pg.

Meteorological parameters were measured by sensors mounted on the EC sampling mast. Global radiation (Rg) was measured at 4 m height using a Li200sz sensor (LICOR, Lincoln, Nebraska, USA). Air temperature (Ta) and humidity (Rh) were determined by a MP100 temperature and moisture sensor (Rotronic AG, Bassersdorf, Switzerland) inside a ventilated radiation shield mounted 1.8 m above the peatland surface. Mean water levels and soil temperatures representative for the REA footprint were measured 100 m northeast of the EC sampling mast. The WTL was measured using a float and counterweight system attached to a potentiometer (Roulet et al., 1991). Soil temperature (Ts) at 2 cm depth was measured by TO3R thermistors mounted in sealed, waterproof, stainless steel tubes (TOJO Skogsteknik, Djäkneboda, Sweden). Due to an instrument failure, Ts data for only 65% of the campaign period were logged. All environmental data were stored as 30 min averages on a data logger (CR10X, Campbell Scientific, Logan, Utah). Air temperature and relative humidity inside and outside (10 cm above surface) the DFC were measured every 5 min by a ELUSB-2 Humidity, Temperature and Dew Point Data Logger on a 5 min base (DATAQ Instruments, Akron, USA).

3. Results and discussion

3.1. Environmental conditions

Meteorological conditions during the campaign were consistently

Table 1
Summary of mean, median and 10th and 90th percentiles of the GEM flux determined with a Teflon® PFA and new type dynamic flux chamber (TDFC and Aero-DFC) and the relaxed eddy accumulation (REA) technique. Simultaneously determined air GEM concentrations (measured with the DFC and REA setup) and environmental parameters are listed. Pearson correlation coefficients (r) between GEM flux and factors controlling GEM flux are given in bold if statistically significant ($p < 0.05$). Number of observations (n) are indicated.

Variable	08.07–12.07.2014									
	unit	Mean	Median	10th/90th %-iles	r_{TDFC}	n	$r_{Aero\text{-}DFC}$	n	r_{REA}	n
TDFC flux	ng m^{-2} h^{-1}	0.66	0.4	−0.77/2.6	[-]	32	[-]	[-]	[-]	[-]
Aero-DFC flux	ng m^{-2} h^{-1}	1.93	0.63	−1.78/7.73	**0.76**	32	[-]	[-]	[-]	[-]
REA flux	ng m^{-2} h^{-1}	2	1.6	−27/34	0.06	96	0.03	96	[-]	96
REA footprint parameters										
GEM concentration REA	ng m^{-3} [3.5 m]	1.3	1.3	1.15/1.46	[-]	[-]	[-]	[-]	−0.02	192
GEM concentration DFCs	ng m^{-3} [20 cm]	1.5	1.57	1.17/1.46	**0.87**	32	**0.75**	32	[-]	[-]
Solar radiation	W m^{-2}	253	208	1.7/559	**0.8**	32	**0.79**	32	−0.01	192
Temperature [2 m]	°C	19.7	20.9	11.1/27.5	**0.81**	32	**0.74**	32	**0.26**	192
Temperature inside TDFC	°C	25.8	32.6	9/39.1	**0.81**	31	[-]	[-]	[-]	[-]
Temperature inside Aero-DFC	°C	22.3	18	7.5/39.2	[-]	[-]	**0.82**	30	[-]	[-]
Temperature outside DFCs	°C [10 cm]	20.2	21.5	8.8/30.1	**0.81**	32	**0.8**	32	[-]	[-]
Soil temperature	°C [-2 cm]	18.5	18.7	14.9/21.7	[-]	[-]	[-]	[-]	**0.51**	127
Relative humidity	%	66.8	64.5	40.7/97.1	**−0.79**	32	**−0.68**	32	**−0.31**	192
Wind speed	m s^{-1}	1.6	1.7	0.3/2.9	**0.42**	32	**0.49**	32	**0.16**	192
Friction velocity	m s^{-1}	0.2	0.2	0.07/0.32	[-]	[-]	[-]	[-]	0.16	192
Mean water level	cm	−15.5	−15.4	−16.6/-14.6	[-]	[-]	[-]	[-]	0.12	127
Substrate Hg [0–10 cm]	ng g^{-1}	23.7	24	20/28	[-]	8	[-]	8	[-]	[-]

very fair and warm for the region (19.7 ± 6.1 °C) (Fig. 3). No precipitation was recorded during the measurements. Nighttime conditions with global radiation below 5 W m^{-2} accounted for 19% of the period. Fog formed during the nights when relative humidity was close to 100%. Wind speed was considerably higher during the day (2.0 ± 1.0 m s^{-1}) than at night (0.9 ± 0.9 m s^{-1}). Prevailing winds were from north (39%) and east (46%) (Fig. 1b).

Atmospheric conditions were stable ($z/L > 0.2$; where z is the measuring height and L the Monin-Obukhov stability length), neutral ($-0.2 < z/L > 0.2$) and unstable ($z/L < 0.2$) during 23%, 8% and 69% of the time, respectively. At nighttime, stable conditions were dominant (64%). 77% of the measurement period featured windy conditions ($u^* > 0.1$ m s^{-1}), during which turbulent transport of GEM is assumed to be predominant.

The mean water table within the REA fetch decreased from 14.2 to 16.6 cm below the surface during the course of the measurements (Fig. 3). The air GEM concentration measured at 3.5 m a.g.l. ranged between 0.9 and 1.7 ng m^{-3} and showed no discernible dependence on wind direction (Fig. 1c). The corresponding mean of 1.3 ± 0.1 ng m^{-3} during the four-day campaign compares with observations made in boreal Fennoscandia (Nerentorp et al., 2013). Thus, to summarize, due to the heatwave present in July 2014, meteorological conditions were very stable during the campaign and ideal for a field inter-comparison of flux measurement methods operating over differing spatio-temporal scales.

3.2. REA flux characteristics

The average ± SD GEM flux measured with REA was 2 ± 24 ng m^{-2} h^{-1} and ranged from −83 to 72 ng m^{-2} h^{-1} (Table 1). The median ± MAD (median absolute deviation) was 1.6 ± 17 ng m^{-2} h^{-1}. Both, average air GEM concentration and turbulent flux were independent of wind direction (Figs. 1c and 2c). The mean concentration difference between up- and downdrafts measured with the gold cartridge pairs C1-C3 and C2-C4 were 0.05 and 0.04 ng m^{-3}, respectively. Even though the concentration gradient was below the detection limit of 0.03 ng m^{-3} for 36% and 59% of the time for the respective gold cartridge pairs, smaller concentration gradients were included in the results, as average fluxes would otherwise be overestimated (Fritsche et al., 2008b).

Based on the REA footprint calculations after Rannik et al. (2000), 80% of the REA GEM flux during the campaign originated from an area of 11500 m^2 (Fig. 1a). The measurement plots in the north (N 1,2), east (E 1,2) and south (S 1,2), were situated within the main wind directions which were from northwest to southeast. The area southwest of the sampling mast contributed only 5% of the GEM source area and was represented by plot (W 1,2). We conclude that GEM exchange from the western part of the peatland was rather underrepresented in the REA signal, while northwestern, northeastern and southeastern areas contributed 23%, 31% and 41% to the GEM source area, respectively (Fig. 2c).

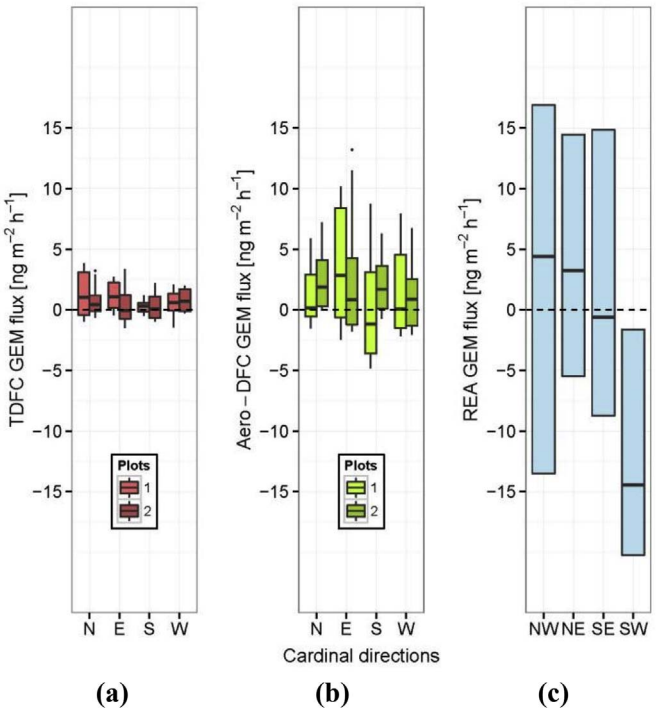

Fig. 2. GEM median fluxes measured with the Teflon® PFA dynamic flux chamber (TDFC) (a) and new type dynamic flux chamber (Aero-DFC) (b) over two plots at each cardinal direction surrounding the relaxed eddy accumulation (REA) system (c) (n = 8 per boxplot). The REA GEM flux is separated in four sectors of wind direction (blue). The N, E, S and W plots were located within the NW, NE, SE, SW wind sectors, respectively. The black bar indicates the median, the top and bottom edges of the boxes indicate the 75th and the 25th percentiles, respectively. The whiskers indicate 1.5 times the interquartile range. Whiskers and outliers (black dots) are not displayed in (c) in order to keep axis scale comparable between the three methods. (For interpretation of the references to colour in this figure legend, the reader is referred to the web version of this article.)

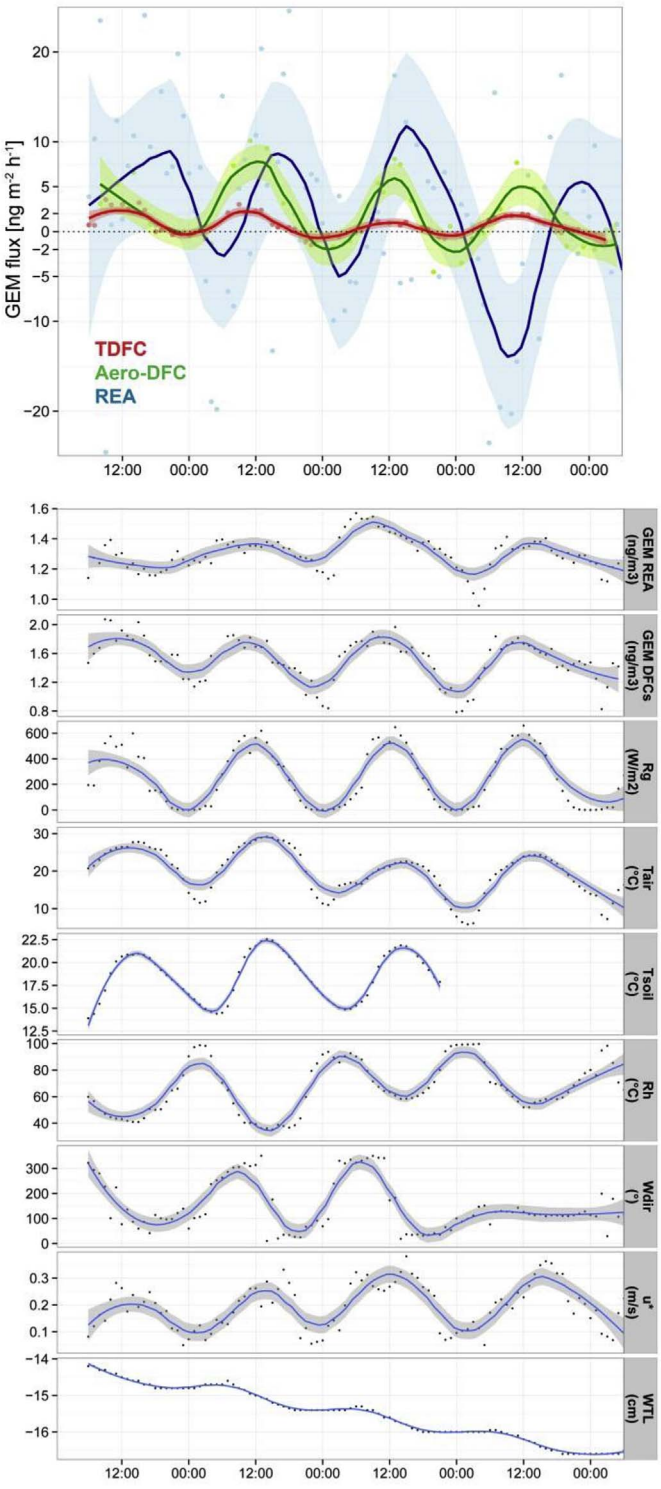

Fig. 3. Time series of GEM fluxes measured with Teflon® PFA dynamic flux chamber (TDFC), new type DFC (Aero-DFC) and the relaxed eddy accumulation (REA) system. Air GEM concentrations derived from both methods (REA and DFCs), global radiation (Rg), air temperature (Tair), soil temperature (Tsoil), relative humidity (Rh), wind direction (°), friction velocity (u*) and water table level (WTL) during the campaign are illustrated. Black dots are hourly averages. Locally weighted scatterplot smoothing (blue line) was applied (R v3.1.2, loess {stats}, span = 0.3) with a confidence interval level of 0.95 (grey band). (For interpretation of the references to colour in this figure legend, the reader is referred to the web version of this article.)

3.3. DFC flux characteristics

The average ± SD of the GEM flux was 0.7 ± 1.3 for the TDFC (n = 32) and 1.9 ± 3.8 for the Aero-DFC (n = 32) (Table 1). Median ± MAD were 0.4 ± 1.3 ng m^{-2} h^{-1} and 0.6 ± 3.2 ng m^{-2} h^{-1}, respectively. The two averages were not significantly different (Mann-Whitney *U* test, $\alpha = 0.05$) but the Aero-DFC flux displayed a higher variance (Fig. 2c). The higher variability in the Aero-DFC flux is not just associated with the correction for atmospheric boundary shear conditions (Eq. (4)) but already exhibited larger median absolute deviation (± 2.6 ng m^{-2} h^{-1}) prior to correction (see Fig. S2 in the supplementary material). Besides methodological bias, spatial heterogeneity of the DFC footprints has been shown to influence the magnitude of the parallel flux measurements (Wallschläger et al., 1999; Gustin and Lindberg, 2000). Within the REA footprint, divergences in peat THg, abundance of vascular plants, water table level and DGM were investigated for every cardinal direction (see Fig. S3 and Table S1 in the supplementary material). In the peatland area north of the flux sampling mast THg in the top 34 cm was 48.7 ng g^{-1} and lower compared to the E (58.0 ng g^{-1}), S (60.4 ng g^{-1}) and W (62.0 ng g^{-1}) plots. In the same area vascular plants were less abundant (32%), water table level in the plots was highest (4.5 cm below the surface), and the pore water DGM concentrations were lowest (28 ng L^{-1}). The THg pool in the soil (0–34 cm) differed considerably in the following order: N (718 µg m^{-2}) < W (801 µg m^{-2}) < S (880 µg m^{-2}) < E (1131 µg m^{-2}). Water table level in the other areas of the peatland was in a similar range (12.5–14.1 cm below the surface), whereas vascular plant coverage was highest (52%) within the plots located in the west. Overall, DGM concentration were highest south (46.2 pg L^{-1}) and east (50.9 pg L^{-1}) of the REA sampling mast. The surface peat water was always supersaturated with DGM in respect of air GEM concentrations during sampling (9 a.m.–4 p.m.). GEM fluxes were averaged for each of the eight plots and inter-compared by analysis of variance (ANOVA, $p < 0.05$). Prior to analysis the response variables were log-normalized to achieve normal distribution. Discernible variability in GEM flux was detected neither between plots nor directions (Fig. 2a and b). Thus, we conclude that the REA footprint is spatially relatively homogenous with respect to GEM source strength.

The higher total variance in the Aero-DFC flux was largely driven by a more pronounced diel pattern (Fig. 3). Reasons for amplification of the rather well-defined temporal pattern with discernible sharp maximum (emission) and shallow minimum (deposition) include:

1) DFC geometry and aerodynamics: The flat, rectangular design of the Aero-DFC ensured a more uniform airflow over the surface and increased airstream velocity. This resulted in thinner surface boundary layer with diminished soil/air exchange resistance advancing GEM emission from the soil. Non-horizontal flow in the TDFC reduced the exchange surface area (Zhang et al., 2002; Eckley et al., 2010; Agnan et al., 2016).
2) DFC air exchange rate: The volume and turnover time for the TDFC was 10 times higher compared to the Aero-DFC. Less voluminous DFCs and shorter turnover times were reported to positively influence GEM emission (Eckley et al., 2010). The Aero-DFC was operated at 13.3 L min^{-1}, which is within the recommended flushing flow rate range based on tests over soil surfaces with a roughness ($< 10^{-2}$ m) similar to the present study (Lin et al., 2012). This also holds for the TDFC since lower flushing flow rates are recommended for much smaller traditional DFCs at background sites (Engle et al., 2006; Eckley et al., 2010). However, the slower turnover time may have created an artificial boundary layer with elevated Hg concentrations at the air-surface interface resulting in a suppression of emissions (Gustin et al., 1999).
3) Fabrication material: The Aero-DFC displayed a slightly higher and more variable blank in comparison to the consistently low TDFC blank. Teflon® PFA film is in addition considered an ideal material

for Hg research DFCs due to its full transmission of actinic light (Eckley et al., 2010). Polycarbonate DFCs in contrast block wavelengths below 320 nm and therefore tend to underestimate GEM fluxes (Eckley et al., 2010). A recent synthesis of GEM flux measurements in Western North America found that fluxes from Teflon® DFCs were 150% higher than fluxes measured using polycarbonate DFCs (Eckley et al., 2016). Nevertheless, DFCs seem not able to preserve ambient air temperature due to altered long-wave radiation balance. On an average, we found a substantially positive difference between inside and outside temperature that is more pronounced for the TDFC (5.3 ± 4.9 °C) compared to the Aero-DFC (2.6 ± 5.7 °C). We presume that the effect is substantially less in terms of surface soil temperature difference and plausibly less grave in perturbing the GEM exchange process at the soil interface.

Bi-directional exchange of GEM was evident with daytime (02:30–21:30) emission and shallow nighttime (22:00–02:00) deposition (Fig. 3). Both the TDFC and Aero-DFC flux data sets showed positive skewness (0.43 and 0.59) due to a sharper daytime peak than the features of nocturnal levelling-off.

3.4. Comparison of REA and DFC measurement techniques

Our results suggest that site heterogeneity was minimal and that thus a direct method comparison was possible because no scaling effect had to be expected. The mean values of GEM fluxes derived from the REA and the Aero-DFC method were not statistically different (Mann-Whitney *U* test, $\alpha = 0.05$) albeit the REA flux had a considerably higher variation (Fig. 3). The highly variable 30 min turbulent fluxes are subject to constant changes of atmospheric turbulence within the surface layer and are typical for MM measurements. The REA flux is considered as net ecosystem Hg flux including GEM emission from the soils, water and vegetation surfaces and dry deposition i.e. GEM uptake by vegetation. The estimated strong influence by atmospheric conditions on the REA flux seems to smear distinct diel patterns gauged by the DFC systems and simultaneously increases overall heterogeneity of fluxes. Surface soil temperature was the only environmental variable strongly positively correlated with REA GEM flux (generally: $r \leq 0.3$, $p < 0.05$). Weak correlations with environmental parameters are most common within MM GEM flux studies (e.g. Fritsche et al., 2008a; Fritsche et al., 2008b; Bash and Miller, 2009; Converse et al., 2010).

Nevertheless, the REA flux indicated net GEM deposition in the early morning hours and predominant GEM emission from midday until after midnight. The drop in GEM emission in the early afternoon probably indicates compensation of elevated GEM volatilization due to solar radiation, air and soil temperature by uptake of GEM by plants (Fig. 3). GEM dry deposition to the peat surface by foliar uptake has been shown to be the dominant deposition pathway in a peat bog in the French Pyrenees (Enrico et al., 2016). In the present study, THg content was considerably higher in moss (Sphagnum species, 77 ± 30 ng g^{-1}) compared to sedges (11 ± 4.4 ng g^{-1}) as was also noted by (Rydberg et al., 2010). Sphagnum moss mats in boreal wetlands are hot spots for Hg accumulation and methylation (Yu et al., 2010). Nevertheless, the mechanism of atmospheric GEM uptake is still unclear especially for moss due to the absence of stomata. Air GEM concentrations measured in the DFC inlet air were 1.5 ± 0.3 ng m^{-3}, and 15% higher compared to REA derived concentrations. This implies the development of a concentration gradient between 0.2 m (DFC measurement) and 3.5 m (REA) a.g.l during sunlight hours (Fig. 3). Air GEM concentrations at 0.2 m above the surface showed a distinct diel pattern with highest median concentrations between 08:00 and 14:00. During the DFC measurements a significant positive correlation between air GEM concentrations and GEM exchange was found ($r = 0.87$ and $r = 0.75$, $p < 0.05$), while most studies report negative correlations (reviewed by Agnan et al., 2016).

Estimated contemporary Hg accumulation rates based on THg in the peat profiles and peat growth rates account for ~4 μg m^{-2} yr^{-1} and is much lower than average Hg accumulation rates from Pinet bog (34 ± 8 m^{-2} yr^{-1}) located in the French Pyrenees (42°52′N, 1°5′E; 880 m a.s.l.) (Enrico et al., 2016) and from other wetlands worldwide (25 μg m^{-2} yr^{-1}) (Amos et al., 2015). In concert with low Hg accumulation rates the flux measurements revealed low GEM dry deposition velocities measured with the TDFC, Aero-DFC and REA of 0.008, 0.012 and 0.043 cm s^{-1}, respectively. Median GEM dry deposition velocities were generally lower than in other DFC studies (< 0.05 cm s^{-1}; Zhang et al., 2009; 0.1 cm s^{-1}; Enrico et al., 2016) and REA studies (< 0.2 cm s^{-1}; Zhu et al., 2015a). Deposition velocities < 0.03 cm s^{-1} indicates hindered GEM deposition and probably low uptake of GEM by plants (Lee et al., 2000). At Degerö, net dry deposition occurred in 41% (TDFC), 38% (Aero-DFC) and 37% (REA) of the measurement period.

In this perspective, the REA flux pattern may reflect coupling with variations in larger scale atmospheric GEM concentrations over the landscape indicated by a maximum rate of change in GEM concentrations of 0.22 ng m^{-3} h^{-1}. Larger, low-frequency flow patterns, i.e. coherent structures, may cause (opposite flux) differences between DFCs and MM measurement results (Riederer et al., 2014).

Long-term measurements conducted at the same site in July 2013 indicate that the short-term REA measurements presented herein are representative for summer time GEM emission rates (Osterwalder et al., in review.). This was the first MM-flux study performed over peatlands with background THg concentrations in the peat of < 0.3 μg g^{-1}. Globally GEM flux measurements performed over background wetlands (n = 23) ranged between −4.8 and 6.6 ng m^{-2} h^{-1} (Agnan et al., 2016).

DFC fluxes followed a distinct diel pattern during the campaign with the change from GEM emission to net deposition occurring between 17:00 and 23:00 (Fig. 3). DFC emission peaked between 11:00 and 14:00 and was in concert with daytime peaks of global radiation, air and soil temperature. Besides these main controlling factors on land-atmosphere exchange of GEM, other meteorological variables, such as relative humidity, wind speed/turbulence and air Hg and oxidant concentrations can also affect GEM exchange (Carpi and Lindberg, 1997; Poissant et al., 1999; Engle et al., 2005; Xin and Gustin, 2007; Sizmur et al., 2017). Pearson correlation coefficients showed a significant positive relationship for both DFCs between GEM flux ($r = 0.76$, $p < 0.05$) and global radiation, air and soil temperature (correlation coefficients are listed in Table 1). A strong negative correlation was found with relative humidity.

Even though DFCs operate decoupled from atmospheric conditions and are subject to measurement artefacts due to the perturbed micro-environment, the cumulative fluxes indicated similar source strength per aerial unit from small Aero-DFC (0.09 m^2) and the larger REA footprints (averaging at 11500 m^2). In contrast, the cumulative flux gauged by the TDFC was just 37% of the Aero-DFC and REA fluxes, which summed up to 175 and 173 ng m^{-2}, respectively (Fig. 4). However, the temporal feature of the REA flux reveals different flux patterns, occasionally in reverse directions, reflecting the inherent variability in the turbulent fluxes (Fig. 5).

Despite this observed flux variability, the mean and magnitude of the REA flux is comparable with the fluxes derived from the Aero-DFC. This indicates that in contrast to the TDFC, the Aero-DFC flux correction with synchronized surface shear properties seem to bridge discrepancies in the magnitude of fluxes gauged between the DFC and REA methods. Since wind speed was comparably low averaging 1.6 ms^{-1} during the campaign we were not able to apply the Aero-DFC flux at high wind speeds, but overall, larger turbulent fluxes and stronger variability are expected at higher wind speeds correspondingly with Aero-DFC fluxes that scales with $(u^*)^{1/3}$. However, DFC measurements remain biased by altering temperature and moisture regimes over the footprint and are insensitive to changes in atmospheric conditions that can control the flux (Lin et al., 2012). The application of DFCs is impeded over tall vegetation and limited during precipitation or snow

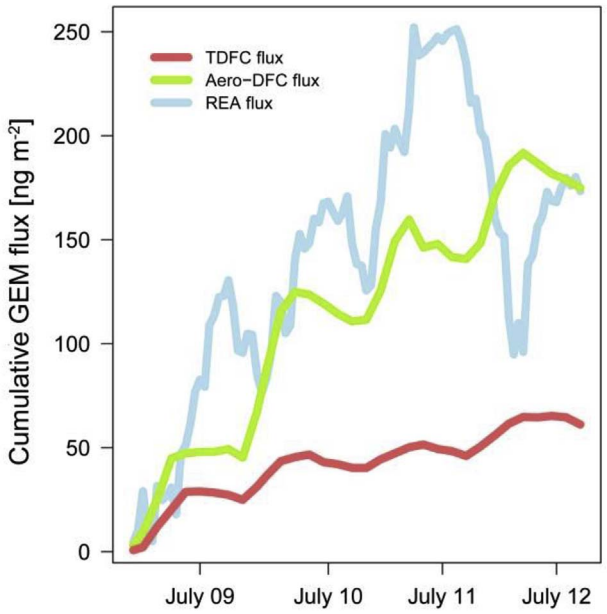

Fig. 4. Time series of the cumulative GEM flux measured with the Teflon® PFA and new type dynamic flux chambers (TDFC and Aero-DFC) and relaxed eddy accumulation (REA) technique.

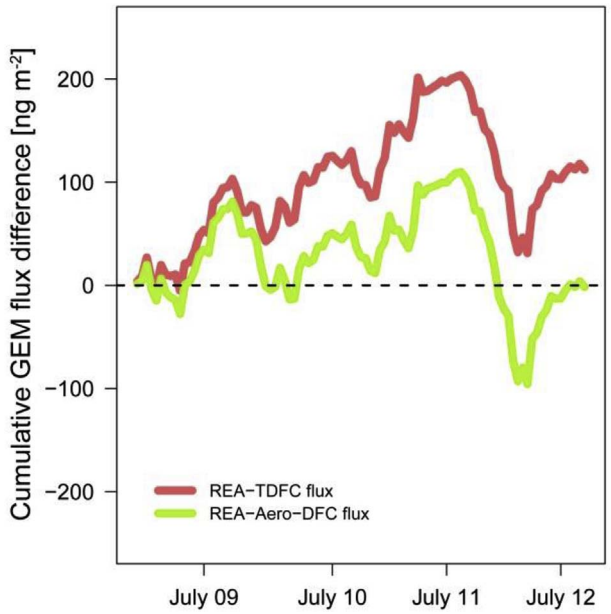

Fig. 5. Cumulative GEM flux difference between the relaxed eddy accumulation (REA) technique and both the Teflon® PFA dynamic flux chamber (TDFC) as well as the new type dynamic flux chamber (Aero-DFC).

events (Hg wet deposition). Prolonged DFC measurements are also supposed to modify GEM uptake by foliage due to influences on plant physiology. To assess net annual Hg exchange on an ecosystem scale, heterogeneity in soil surface characteristics has to be addressed with spatially and temporally repeated measurements.

In a boreal peatland with a pronounced seasonal climate, many DFC measurement campaigns under different meteorological conditions and subsequently a high demand for manpower would be necessary to upscale a quantitative flux based on field measurements. It is likely that Aero-DFC and REA only measure comparable fluxes in spatially homogeneous areas, but that in heterogeneous environments a larger number of DFC measurements would be necessary to represent the landscape, which means that REA in the end might be the more reliable or, depending on analytical and staff availability even the more convenient method. To rule out the possibility that means and magnitudes of the REA and Aero-DFC flux were similar by coincidence we suggest prolonged method inter-comparison campaigns under varying meteorological conditions. Thus, concurrent measurements with DFCs, REA and other MM-methods under changing environmental conditions are required to define methodological bias and to derive a standard protocol for flux measurements.

4. Conclusions

In this study we compared quantitative summertime GEM flux exchange over a boreal peatland using a TDFC, Aero-DFC and the novel dual-inlet, single detector REA system during four consecutive days. A method inter-comparison was propitious, because of very stable weather conditions and homogenous vegetation cover. Thus, alternate DFC measurements identified the REA footprint as a homogeneous GEM source area independent of small-scale changes in topsoil THg concentration, abundance of vascular plants, water table levels or dissolved gaseous mercury concentrations in the peat pore water. Daily average GEM flux for the three methods displayed depositional features during dark hours, which after dusk shifted to efflux gradually progressing towards a day-time maximum. The temporal variation in the measured fluxes among the three deployed methods increased in the sequence TDFC < Aero-DFC < REA. DFC time series showed distinct diel patterns indicating that repetitive 24 h measurements are necessary for quantitative DFC estimates on an ecosystem scale. Diel patterns were not detected by REA most likely due to the GEM flux correlation to climatic conditions which overprinted possible diel emission dynamic.

Spatial repetition of DFC measurements indicated very homogenous GEM flux emission patterns under the consistent weather conditions during our measurement period. Due to these consistent weather conditions and the spatial homogeneity of the peat surface, the Aero-DFC technique measured cumulative fluxes similar to the turbulent fluxes obtained by REA. This indicates that the Aero-DFC has the technical potential to bridge the gap in GEM flux magnitude frequently reported between turbulent and enclosure-based measurements We expect that the novel REA design is not subject to significant flux overestimation (as was concluded by Zhu et al., 2015a for another REA design). However, to identify landscape-specific GEM sink-source characteristics REA should be applied in long-term measurement campaigns that allow temporal and spatial flux averaging. Caution must be taken in the interpretation of short-term REA fluxes especially during periods when GEM concentration difference in updrafts and downdrafts are small. For short-term and small spatial scale, mechanistic studies DFCs are the favorable tool with the Aero-DFC suitable for quantitative flux estimations over low vegetation in homogenous environments.

Acknowledgements

We thank the Swiss National Foundation (Doc.Mobility fellowship #P1BSP2_148458) and the Swedish Research Council (SMAREF Multi-project grant #639-2013-6978) for financing this project. We would like to acknowledge the crew of the field-based forest research station in Vindeln for using their research infrastructure and to make meteorological and soil data available. The study was also supported by ICOS Sweden (Integrated Carbon Observatory System) and SITES (Swedish Infrastructure for Ecosystem Science) at Degerö Stormyr, both partly financed by the Swedish Research Council.

Appendix A. Supplementary data

Supplementary data related to this article can be found at http://dx.doi.org/10.1016/j.atmosenv.2017.10.025.

References

Agnan, Y., Le Dantec, T., Moore, C.W., Edwards, G.C., Obrist, D., 2016. New constraints on terrestrial surface-atmosphere fluxes of gaseous elemental mercury using a global database. Environ. Sci. Technol. 50, 507–524.

Amos, H.M., Sonke, J.E., Obrist, D., Robins, N., Hagan, N., Horowitz, H.M., Mason, R.P., Witt, M., Hedgecock, I.M., Corbitt, E.S., Sunderland, E.M., 2015. Observational and modeling constraints on global anthropogenic enrichment of mercury. Environ. Sci. Technol. 49, 4036–4047.

Bash, J.O., Miller, D.R., 2008. A relaxed eddy accumulation system for measuring surface fluxes of total gaseous mercury. J. Atmos. Ocean. Technol. 25, 244–257.

Bash, J.O., Miller, D.R., 2009. Growing season total gaseous mercury (TGM) flux measurements over an *Acer rubrum* L. stand. Atmos. Environ. 43, 5953–5961.

Baya, A.P., Van Heyst, B., 2010. Assessing the trends and effects of environmental parameters on the behaviour of mercury in the lower atmosphere over cropped land over four seasons. Atmos. Chem. Phys. 2010 (10), 8617–8628.

Bergman, I., Bishop, K., Tu, Q., Frech, W., Åkerblom, S., Nilsson, M., 2012. The influence of sulphate deposition on the seasonal variation of peat pore water methyl Hg in a Boreal Mire. PLoS One 7. http://dx.doi.org/10.1371/journal.pone.0045547.

Carpi, A., Lindberg, S.E., 1997. Sunlight-mediated emission of elemental mercury from soil amended with municipal sewage sludge. Environ. Sci. Technol. 31, 2085–2091.

Cobos, D.R., Baker, J.M., Nater, E.A., 2002. Conditional sampling for measuring mercury vapor fluxes. Atmos. Environ. 36, 4309–4321.

Converse, A.D., Riscassi, A.L., Scanlon, T.M., 2010. Seasonal variability in gaseous mercury fluxes measured in a high-elevation meadow. Atmos. Environ. 44, 2176–2185.

Eckley, C.S., Gustin, M., Lin, C.-J., Li, X., Miller, M.B., 2010. The influence of dynamic chamber design and operating parameters on calculated surface-to-air mercury fluxes. Atmos. Environ. 44, 194–203.

Eckley, C.S., Tate, M.T., Lin, C.-J., Gustin, M., Dent, S., Eagles-Smith, C., Lutz, M.A., Wickland, K.P., Wang, B., Gray, J.E., Edwards, G.C., Krabbenhoft, D.P., Smith, D.B., 2016. Surface-air mercury fluxes across Western North America: a synthesis of spatial trends and controlling variables. Sci. Total Environ. http://dx.doi.org/10.1016/j.scitotenv.2016.02.121.

Edwards, G.C., Rasmussen, P.E., Schroeder, W.H., Wallace, D.M., Halfpenny-Mitchell, L., Dias, G.M., Kemp, R.J., Ausma, S., 2005. Development and evaluation of a sampling system to determine gaseous Mercury fluxes using an aerodynamic micrometeorological gradient method. J. Geophys Res-Atmos. http://dx.doi.org/10.1029/2004JD005187.

Engle, M.A., Gustin, M.S., Lindberg, S.E., Gertler, A.W., Ariya, P.A., 2005. The influence of ozone on atmospheric emissions of gaseous elemental mercury and reactive gaseous mercury from substrates. Atmos. Environ. 39, 7506–7517.

Engle, M.A., Gustin, M.S., Goff, F., Counce, D.A., Janik, C.J., Bergfeld, D., Rytuba, J.J., 2006. Atmospheric mercury emissions from substrates and fumaroles associated with three hydrothermal systems in the western United States. J. Geophys. Res.-Atmos 111, D17304. http://dx.doi.org/10.1029/2005JD006563.

Enrico, M., Le Roux, G., Marusczak, N., Heimburger, L.-E., Claustres, A., Fu, X., Sun, R., Sonke, J.E., 2016. Atmospheric mercury transfer to peat bogs dominated by gaseous elemental mercury dry deposition. Environ. Sci. Technol. http://dx.doi.org/10.1021/acs.est.5b06058.

Fritsche, J., Wohlfahrt, G., Ammann, C., Zeeman, M., Hammerle, A., Obrist, D., Alewell, C., 2008a. Summertime elemental mercury exchange of temperate grasslands on an ecosystem-scale. Atmos. Chem. Phys. 8, 7709–7722.

Fritsche, J., Obrist, D., Zeeman, M.J., Conen, F., Eugster, W., Alewell, C., 2008b. Elemental mercury fluxes over a sub-alpine grassland determined with two micrometeorological methods. Atmos. Environ. 42, 2922–2933.

Fritsche, J., Osterwalder, S., Nilsson, M.B., Sagerfors, J., Åkerblom, S., Bishop, K., Alewell, C., 2014. Evasion of elemental mercury from a boreal peatland suppressed by long-term sulfate addition. Environ. Sci. Technol. 1, 421–425.

Gustin, M.S., Lindberg, S.E., 2000. Assessing the contribution of natural sources to the global mercury cycle: the importance of intercomparing dynamic flux measurements. Fresenius J. Anal. Chem. 366, 417–422.

Gustin, M.S., Lindberg, S., Marsik, F., Casimir, A., Ebinghaus, R., Edwards, G., Hubble-Fitzgerald, C., Kemp, R., Kock, H., Leonard, T., London, J., Majewski, M., Montecinos, C., Owens, J., Pilote, M., Poissant, L., Rasmussen, P., Schaedlich, F., Schneeberger, D., Schroeder, W., Sommar, J., Turner, R., Vette, A., Wallschlaeger, D., Xiao, Z., Zhang, H., 1999. Nevada STORMS project: measurement of mercury emissions from naturally enriched surfaces. J. Geophys. Res.-Atmos 104, 21831–21844.

Kamp, J., Skov, H., Jensen, B., Sørensen, L.L., 2017. Fluxes of gaseous elemental mercury (GEM) in the High Arctic during atmospheric mercury depletion events (AMDEs). Atmos. Chem. Phys. Discuss. 2017, 1–21.

Kyllönen, K., Hakola, H., Hellen, H., Korhonen, M., Verta, M., 2012. Atmospheric mercury fluxes in a Southern Boreal Forest and Wetland. Water Air Soil Pollut. 223, 1171–1182.

Laine, A.M., Bubier, J., Riutta, T., Nilsson, M.B., Moore, T.R., Vasander, H., Tuittila, E.S., 2012. Abundance and composition of plant biomass as potential controls for mire net ecosytem CO_2 exchange. Botany 90, 63–74.

Laudon, H., Taberman, I., Ågren, A., Futter, M., Ottosson-Löfvenius, M., Bishop, K., 2013. The Krycklan catchment study – a flagship infrastructure for hydrology, biogeochemistry, and climate research in the boreal landscape. Water Resour. Res. 49, 7154–7158.

Leach, J.A., Larsson, A., Wallin, M.B., Nilsson, M.B., Laudon, H., 2016. Twelve year interannual and seasonal variability of stream carbon export from a boreal peatland catchment. J. Geophys. Res. Biogeosci. 121. http://dx.doi.org/10.1002/2016JG003357.

Lee, D.S., Nemitz, E., Fowler, D., Hill, P., Clegg, S., Kingdon, R.D., 2000. Sources, Sinks and Levels of Atmospheric Mercury in the UK. Rep.DERA/AS/PTD/CR000114, Farnborough, UK. URL: http://uk-air.defra.gov.uk/library/reports?report_id=102 [last access: 25 October 2017].

Lin, C.-J., Zhu, W., Li, X., Feng, X., Sommar, J., Shang, L., 2012. Novel dynamic flux chamber for measuring air-surface exchange of Hg0 from soils. Environ. Sci. Technol. 46, 8910–8920.

Lindberg, S.E., Kim, K.-H., Meyers, T.P., Owens, J.G., 1995. Micrometeorological gradient approach for quantifying air/surface exchange of mercury vapor: tests over contaminated soils. Environ. Sci. Technol. 29, 126–135.

Lindberg, S.E., Vette, A.F., Miles, C., Schaedlich, F., 2000. Mercury speciation in natural waters: measurement of dissolved gaseous mercury with a field analyzer. Biogeochemistry 48, 237–259.

Lindberg, S.E., Dong, W.J., Meyers, T., 2002. Transpiration of gaseous elemental mercury through vegetation in a subtropical wetland in Florida. Atmos. Environ. 36, 5207–5219.

McMillen, R.T., 1988. An Eddy-correlation technique with extended applicability to non-simple terrain. Bound.-Layer Meteor. 43, 231–245.

Mitchell, C.P.J., Branfireun, B.A., Kolka, R.K., 2008. Spatial characteristics of methylmercury production hot spots in peatlands. Environ. Sci. Technol. 42, 1010–1016.

Nacht, D.M., Gustin, M.S., 2004. Mercury emissions from background and altered geologic units throughout Nevada. Water, Air, Soil Pollut. 151, 179–193.

Nerentorp, M., Kyllönen, K., Wängberg, I., Kuronen, P., 2013. Speciation measurements of airborne mercury species in northern Finland; evidence for long range transport of air masses depleted in mercury. E3S Web Conf. 1, 27003.

Nilsson, M., Sagerfors, J., Buffam, I., Laudon, H., Eriksson, T., Grelle, A., Klemedtsson, L., Weslien, P., Lindroth, A., 2008. Contemporary carbon accumulation in a boreal oligotrophic minerogenic mire - a significant sink after accounting for all C-fluxes. Glob. Change Biol. 14, 2317–2332.

Obrist, D., Conen, F., Vogt, R., Siegwolf, R., Alewell, C., 2006. Estimation of Hg0 exchange between ecosystems and the atmosphere using 222Rn and Hg0 concentration changes in the stable nocturnal boundary layer. Atmos. Environ. 40, 856–866.

Olofsson, M., Sommar, J., Ljungstrom, E., Andersson, M., Wängberg, I., 2005. Application of relaxed eddy accumulation technique to quantify Hg0 fluxes over modified soil surfaces. Water Air Soil Pollut. 167, 331–352.

Osterwalder, S., Bishop, K., Alewell, C., Fritsche, J., Laudon, H., Åkerblom, S., Nilsson, M. B., in review. Mercury from a boreal peatland: Time to rethink timelines for global recovery?.

Osterwalder, S., Fritsche, J., Alewell, C., Schmutz, M., Nilsson, M.B., Jocher, G., Sommar, J., Rinne, J., Bishop, K., 2016. A dual-inlet, single detector relaxed eddy accumulation system for long-term measurement of mercury flux. Atmos. Meas. Tech. 9, 509–524.

Ottosson-Löfvenius, M., Kluge, M., Lundmark, T., 2003. Snow and soil frost depth in two types of shelterwood and a clear-cut area. Scand. J. For. Res. 18, 54–63.

Pierce, A.M., Moore, C.W., Wohlfahrt, G., Hörtnagl, L., Kljun, N., Obrist, D., 2015. Eddy covariance flux measurements of gaseous elemental mercury using cavity ring-down spectroscopy. Environ. Sci. Technol. 49, 1559–1568.

Poissant, L., Pilote, M., Casimir, A., 1999. Mercury flux measurements in a naturally enriched area: correlation with environmental conditions during the Nevada Study and Tests of the Release of Mercury from Soils (STORMS). J. Geophys. Res.-Atmos 104, 21845–21857.

Poissant, L., Pilote, M., Xu, X.H., Zhang, H., Beauvais, C., 2004. Atmospheric mercury speciation and deposition in the Bay St. Francois wetlands. J. Geophys. Res.-Atmos. 109, D11301. http://dx.doi.org/10.1029/2003JD004364.

Rannik, U., Aubinet, M., Kurbanmuradov, O., Sabelfeld, K.K., Markkanen, T., Vesala, T., 2000. Footprint analysis for measurements over a heterogeneous forest. Bound.-Lay. Meteorol. 97, 137–166.

Richardson, A.D., Aubinet, M., Barr, A.G., Hollinger, D.Y., Ibrom, A., Lasslop, G., Reichstein, M., 2012. Uncertainty quantification. In: Aubinet, M., Vesala, T., Papale, D. (Eds.), Eddy Covariance – a Practical Guide to Measurement and Data Analysis. Springer Science + Business Media B.V., Dordrecht, the Netherlands, pp. 173–209.

R Development Core Team, 2011. R: a Language and Environment for Statistical Computing. the R Foundation for Statistical Computing, Vienna, Austria ISBN: 3-900051-07-0, available at: http://www.R-project.org/ [last access: 25 October 2017].

Riederer, M., Serafimovich, A., Foken, T., 2014. Net ecosystem CO_2 exchange measurements by the closed chamber method and the eddy covariance technique and their dependence on atmospheric conditions. Atmos. Meas. Tech. 7, 1057–1064.

Roulet, N., Hardill, S., Comer, N., 1991. Continuous measurement of the depth of water table (inundation) in wetlands with fluctuating surfaces. Hydrol. Process 5, 399–403.

Rydberg, J., Karlsson, J., Nyman, R., Wanhatalo, I., Nathe, K., Bindler, R., 2010. Importance of vegetation type for mercury sequestration in the northern Swedish mire. Rodmossamyran. Geochimica Cosmochimica Acta 74, 7116–7126.

Sagerfors, J., Lindroth, A., Grelle, A., Klemedtsson, L., Weslien, P., Nilsson, M., 2008. Annual CO_2 exchange between a nutrient-poor, minerotrophic, boreal mire and the atmosphere. J. Geophys. Res.-Biogeosci. 113. http://dx.doi.org/10.1029/2006JG000306.

Selin, N.E., Jacob, D.J., Yantosca, R.M., Strode, S., Jaeglé, L., Sunderland, E.M., 2008. Global 3-D land-ocean-atmosphere model for mercury: present-day versus pre-industrial cycles and anthropogenic enrichment factors for deposition. Glob. Biogeochem. Cycles 22, GB2011. http://dx.doi.org/10.1029/2007GB003040.

Selvendiran, P., Driscoll, C.T., Montesdeoca, M.R., Bushey, J.T., 2008. Inputs, storage, and transport of total and methyl mercury in two temperate forest wetlands. J. Geophys. Res. 113, G00C01.

Sigler, J.M., Lee, X., 2006. Gaseous mercury in background forest soil in the northeastern United States. J. Geophys. Res. 2006 (111), G02007. http://dx.doi.org/10.1029/2005JG000106.

Sizmur, T., McArthur, G., Risk, D., Tordon, R., O'Driscoll, N.J., 2017. Gaseous mercury flux from salt marshes is mediated by solar radiation and temperature. Atmos. Environ. 153, 117–125.

Sommar, J., Zhu, W., Shang, L., Feng, X., Lin, C.-J., 2013. A whole-air relaxed eddy accumulation measurement system for sampling vertical vapour exchange of elemental mercury. Tellus B 65, 19940. http://dx.doi.org/10.3402/tellusb.v65i0.19940.

St Louis, V., Rudd, J., Kelly, C., Beaty, K., Bloom, N., Flett, R., 1994. Importance of Wetlands as sources of methyl mercury to boreal forest ecosystems. Can. J. Fish. Aquat. Sci. 51, 1065–1076.

Wallschläger, D., Turner, R.R., London, J., Ebinghaus, R., Kock, H.H., Sommar, J., Xiao, Z.F., 1999. Factors affecting the measurement of mercury emissions from soils with flux chambers. J. Geophys. Res.-Atmos 104, 21859–21871.

Wang, X., Lin, C.-J., Feng, X., 2014. Sensitivity analysis of an updated bidirectional air-surface exchange model for elemental mercury vapor. Atmos. Chem. Phys. 14, 6273–6287.

Wiedermann, M.M., Nordin, A., Gunnarsson, U., Nilsson, M.B., Ericson, L., 2007. Global change shifts vegetation and plant-parasite interactions in a boreal peatland. Ecology 88, 454–464.

Xiao, Z.F., Munthe, J., Schroeder, W.H., Lindqvist, O., 1991. Vertical fluxes of volatile mercury over forest soil and lake surfaces in Sweden. Tellus B 43, 267–279. http://dx.doi.org/10.3402/tellusb.v43i3.15274.

Xin, M., Gustin, M.S., 2007. Gaseous elemental mercury exchange with low mercury containing soils: investigation of controlling factors. Appl. Geochem 22, 1451–1466.

Yu, R.-Q., Adatto, I., Montesdeoca, M.R., Driscoll, C.T., Hines, M.E., Barkay, T., 2010. Mercury methylation in Sphagnum moss mats and its association with sulfate-reducing bacteria in an acidic Adirondack forest lake wetland. Fems Microbiol. Ecol. 74, 655–668.

Zhang, H., Lindberg, S.E., Barnett, M.O., Vette, A.F., Gustin, M.S., 2002. Dynamic flux chamber measurement of gaseous mercury emission fluxes over soils. Part 1: simulation of gaseous mercury emissions from soils using a two-resistance exchange interface model. Atmos. Environ. 36, 835e846.

Zhang, L.M., Wright, L.P., Blanchard, P., 2009. A review of current knowledge concerning dry deposition of atmospheric mercury. Atmos. Environ. 43, 5853–5864.

Zhu, W., Sommar, J., Lin, C.-J., Feng, X., 2015a. Mercury vapor air–surface exchange measured by collocated micrometeorological and enclosure methods – Part I: data comparability and method characteristics. Atmos. Chem. Phys. 15, 685–702.

Zhu, W., Sommar, J., Lin, C.-J., Feng, X., 2015b. Mercury vapor air–surface exchange measured by collocated micrometeorological and enclosure methods – Part II: bias and uncertainty analysis. Atmos. Chem. Phys. 15, 5359–5376.